


Perfect intrinsic and nonlinear chirality simultaneously driven by half-integer topological chargeShijie Cai¹,[✉] Jiafei Chen,¹ Xiaoshan Liu,¹ Guolan Fu,¹ Guiqiang Liu,^{1,*} Jing Chen,² Chaojun Tang,³ Wei Du,⁴ and Zhengqi Liu^{1,†}¹College of Physics and Communication Electronics, Jiangxi Normal University, Nanchang 330022, Jiangxi, China²College of Electronic and Optical Engineering, Nanjing University of Posts and Telecommunications, Nanjing 210023, China³College of Science, Zhejiang University of Technology, Hangzhou 310023, China⁴College of Physics Science and Technology, Yangzhou University, Yangzhou 225002, China (Received 14 December 2023; revised 18 March 2024; accepted 25 March 2024; published 10 April 2024)

Bound states in the continuum hold extraordinary optical topological properties and can significantly enhance the interaction between light and matter including the circular dichroism (CD) in chiral resonant metasurfaces. In this paper, we demonstrate the split and displacement of topological charges through tilted double-elliptical half-disk metasurfaces. It enables the feasibility to attain perfect intrinsic chiroptic responses, with a CD exceeding 0.99. The ellipticity (χ) of the intrinsic chiroptic response, induced by vertical incidence, is also ~ 1 . In addition to linear chirality CD, significant near-field enhancement contrast is observed at the positions of half-integer topological charge, leading to remarkable nonlinear CD approaching a nearly perfect value of 1. The proposed metasurface simultaneously possesses perfect intrinsic chirality and nonlinear chirality, providing an avenue for the multifaceted development of planar optical devices.

DOI: [10.1103/PhysRevB.109.165420](https://doi.org/10.1103/PhysRevB.109.165420)**I. INTRODUCTION**

Chirality is a fundamental property of objects, describing the inability of an object to be superimposed onto its mirror image through geometric translation. Chiral structures are ubiquitous in chemistry, biology, and daily life, whether at the macro scale, such as the spiral structure of the universe and galaxies and shells, or at the micro scale, such as spirulina, amino acids, and DNA [1–5]. It is not only a structural feature of many molecules but also a prerequisite for many evolutions in nature, so studying chirality has broad and important significance in science and engineering. In optics, chirality manifests as chiroptical effects. Unique differences in intensity and phase responses can occur [6,7] when a chiral object interacts with left-circularly polarized (LCP) and right-circularly polarized (RCP) light. The difference in the total transmission of LCP and RCP is commonly described as the circular dichroism (CD) of the object [8,9]. However, the optical chiral response in natural materials is often weak and challenging to be observed. In recent years, with the rapid development of nanofabrication techniques, artificial nanomaterials have provided opportunities for optical chirality [10]. These nanomaterials can guide and enhance optical chiral responses. Several research reports have pointed out that complex three-dimensional (3D) twisted structures or multilayer structures can achieve optical chirality by breaking multiple mirror symmetries [11,12]. However, fabricating these structures often requires highly precise control over manufacturing tolerances and interlayer structures, posing challenges for current nanofabrication technologies.

In recent years, there has been growing interest in the optical chirality generated by two-dimensional (2D) chiral metasurfaces. Compared with 3D metamaterials, such metasurfaces are easier to manufacture while retaining exceptional capabilities in manipulating the propagation of light waves. Typically, high CD can be achieved in metasurfaces by breaking the mirror symmetry within the structural plane and introducing external configurations (oblique incidence). Chirality is inherently a 3D property, and 2D planes cannot break their out-of-plane mirror symmetry. Chirality is relatively weak in single-layer metasurfaces. Recent studies have also suggested that the observed optical chirality effects are realized in nonintrinsically chiral structures [13–16], referred to as extrinsic chirality (pseudochirality) [17]. The chiroptical effects may be observed as long as the arrangement of these metasurfaces cannot be simply superimposed on its mirror symmetry axial plane [18,19]. However, with a few exceptions [20,21], due to considerations of symmetry and Lorentz reciprocity [22,23], transformations of any chiral light are possible even if the metasurfaces exhibit CD in this process. It leads to the emitted light typically being in elliptically polarized states [22,24–27]. Clearly, such external chirality has certain limitations in practical applications.

The unique topological polarization properties of bound states in the continuum (BICs) provide a research platform in the field of nanophotonics. BICs are considered dark states existing in the radiation continuum with an infinite quality factor [28]. This concept originated in the framework of quantum mechanics and was later extended and applied to various wave systems in classical physics. BICs can be formed through precisely designed periodic nanostructures. In essence, there are multiple modes of interference cancellation inside a quantum well, identified as a vortex polarization singularity (V point) in topological optics, which remains unobservable in the far

*liuqg@jxnu.edu.cn

†zliu@jxnu.edu.cn

field [29–33]. By introducing external perturbations such as oblique incidence and breaking the in-plane symmetry of the structure, a radiative channel coupled to free space can be introduced, leading to resonances with high quality factors (Q factors). It is called quasi-BIC (q-BIC) mode, often resulting in features like Fano resonances or electromagnetic-induced transparency in the spectrum [34,35]. Recently, Chen *et al.* [17] discovered that photonic crystal slabs created through tilted trapezoidal etching can move specific polarization singularities in the momentum space system of BICs, enabling the realization of intrinsic chirality in a relatively simple manner. On the other hand, q-BICs enable photon localization, providing an excellent platform for manipulating light-matter interactions [36]. This characteristic has found wide applications in various fields, including the enhanced optical chiral emission [37,38] and chiral nonlinear effects [39–42].

In this paper, we propose a chiral metasurface with intrinsic chirality composed of two silicon elliptical half-disks arranged in a dimer configuration with tilted etching design. Based on the topological properties of BICs, the in-plane C_2^z symmetry and out-of-plane mirror symmetry of the structure can be broken simultaneously by controlling the axial length of the semiellipse and the tilted metasurface, thereby achieving the splitting and displacement of topological charges, thus giving the metasurface excellent intrinsic chiral effects. At positions corresponding to half-integer topological charges (C points), the CD values exceed 0.99, and the ellipticity of the intrinsic chirality obtained under normal incidence approaches 1. By reversing the tilt direction, the sign of CD can be changed to obtain different chiral responses. Particularly, owing to the unique properties of the C point in the q-BIC, the metasurfaces exhibit huge nonlinear CD. At the C point resonance positions, the nonlinear CDs for both the third harmonic generation (THG) and fifth harmonic generation (FHG) approach 1. The results provide an avenue for simultaneously achieving intrinsic and nonlinear chirality and can be expected for chiral light sources and detectors, chiral sensing, and other fields.

II. RESULTS AND DISCUSSION

A. Structure and model

The chiral metasurface considered is illustrated in Fig. 1, consisting of periodically arranged Si double-elliptical half-disks on an SiO₂ substrate. The refractive indices of Si and SiO₂ are referred to as the data indicated in the Palik handbook. Above the metasurfaces, there is a layer of electron-beam resist [polymethyl methacrylate (PMMA)] to maintain refractive index symmetry in the environment above and below the metasurfaces. In this paper, three sets of metasurfaces with different parameters have been designed to systematically investigate the half-integer topological charges with the purpose of simultaneously driving intrinsic and nonlinear chirality. We conducted numerical simulations using the wave optics module in the COMSOL Multiphysics simulation software. Following the simulation method described in Refs. [40,43], a wavelength-domain solver was employed in this process to calculate the spectrum of the metasurface, with the silicon metasurface placed within a rectangular spatial

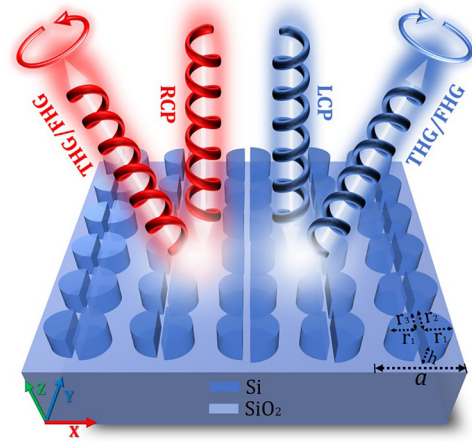


FIG. 1. Schematic diagram of the planar silicon metasurface, consisting of double-elliptical half-disk dimer unit cells on a quartz substrate. Circularly polarized light is incident along the z direction, perpendicular to the surface. The bottom right corner displays the basic parameters of a single unit cell. Geometric parameters: Period $a = 800$ nm, distance between the left and right elliptical half-disks is 50 nm, height $h = 260$ nm, major axis $r_1 = 295$ nm, and initial minor axes $r_2 = r_3 = 235$ nm.

domain. Circular polarization excitations and detection ports were set on both sides in the z direction, where incident waves were generated as RCP and LCP waves through periodic ports 1 and 2 at the top of the modeling domain. These ports also recorded reflected LCP and RCP waves. Detectors at the bottom of the domain (periodic ports 3 and 4) recorded the transmitted RCP and LCP waves. Additionally, perfect matching layers were added as boundary conditions, serving as absorbing media to ensure no spatial reflection of electromagnetic waves at all frequencies and incident angles. Continuous distributed Floquet periodic boundary conditions were set up in the x and y directions to simulate the replication of the infinite planar array of unit cells and compensate for phase differences under oblique illumination. Furthermore, we utilized the eigenfrequency solver to calculate the eigenmodes and Stokes parameters of the planar silicon metasurface, thus simulating the process of splitting and displacement of topological charges. The results obtained from these two solvers can be mutually validated.

B. Intrinsic chirality empowered by half-integer topological charges

To analyze its chiral physical origin, an eigenfrequency solver is used to compute the modal characteristics of the metasurface in momentum space. When the short axes of the two elliptical half-disks on the metasurface are equal, satisfying the in-plane inversion symmetry $(x, y) \rightarrow (-x, -y)$, the band structure and Q factor are shown in Fig. 2(a). Clearly, the metasurface can support an ideal symmetrically protected BIC with an infinite Q factor at the Γ point ($k_x = k_y = 0$). At this point, the Γ -BIC is entirely embedded in the continuum, corresponding to specific high-symmetry points in reciprocal space. This can be described as interference cancellation

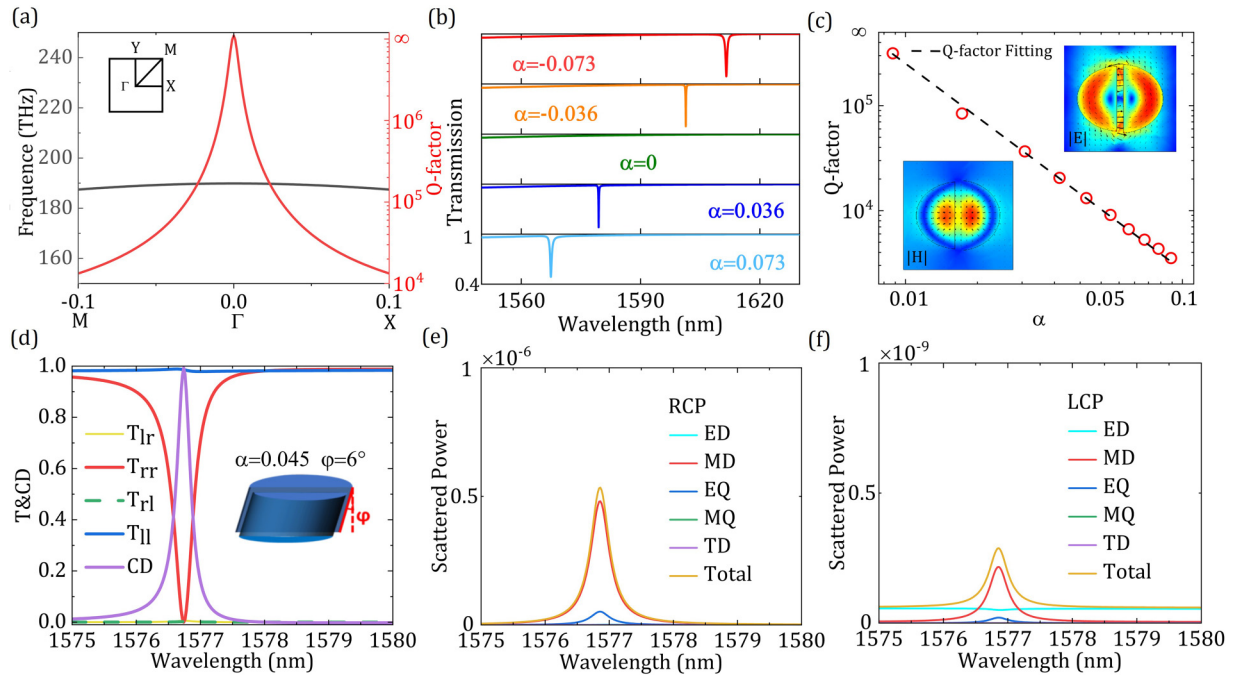


FIG. 2. (a) The band structure and associated Q factors of the metasurface composed of double-elliptical half-disks along the $M\text{-}\Gamma\text{-}X$ ($k_x a/2\pi$) direction. (b) Transmittance spectra for different geometric asymmetry parameters α . (c) Resonant Q factors and their dependence on geometric asymmetry parameter α , with a fitting of the inverse quadratic law shown by the black dashed line. Insets in the top right and bottom left corners depict the normalized electric field ($|E|$) and magnetic field ($|H|$) distributions dominated by the magnetic dipole (MD) mode under the q-BIC mode. (d) Maintaining the geometric asymmetry parameter α at 0.045, the transmission spectrum and circular dichroism (CD) spectrum obtained by tilting the double-elliptical half-disk unit cells ($\varphi = 6^\circ$), where T_{rr} , T_{lr} , T_{ll} , and T_{rl} are the transmission components defined by the Jones matrix, and the inset illustrates the direction of the tilted metasurface. (e) and (f) Contributions of electric dipole (ED), MD, electric quadrupole (EQ), magnetic quadrupole (MQ), and toroidal dipole (TD) to the far-field radiation for right-circularly polarized (RCP) and left-circularly polarized (LCP) incidences.

occurring in a mixed system composed of continuous and discrete states, rendering it unobservable in the far field. By shortening one of the ellipse short axes (r_3), the C_2^z symmetry of the metasurfaces is broken, defining the geometric asymmetry parameter as the ratio of the perturbed area to the initial area $\alpha = \Delta S/S$, where $\Delta S = \pi r_1(r_2 - r_3)$ and $S = \pi r_1 r_2$. Figure 2(b) illustrates the relationship between the transmission spectrum and α . When $\alpha \neq 0$, the radiative channel of the BIC opens due to structural symmetry mismatch, and the BIC collapses into a q-BIC coupled to free-space radiation. As α increases, the resonance linewidth gradually increases. Figure 2(c) also illustrates the relationship between the Q factors and α . The well-fitted results closely follow the expected law of $Q \sim \alpha^{-2}$, which is a distinctive feature of the q-BIC metasurface. This confirms that the symmetry-breaking approach aligns with the established BIC framework driven by C points in chiral configurations. It is noteworthy that, at this point, the q-BIC state is like most 2D metasurface-supporting q-BICs. Although it breaks the inversion symmetry (in-plane C_2^z symmetry), there is still a mirror plane (σ_z symmetry) perpendicular to the surface normal, making them geometrically nonchiral and resulting in no optical chirality response. At this point, by tilting the 2D metasurface along the y direction, the remaining mirror symmetry of the metasurface is broken, where the tilting angle is defined as φ . This additional tilt introduces a perturbation and disrupts the σ_z symmetry of the metasurface, endowing it with customizable intrinsic

chirality. Figure 2(d) shows the transmission and CD spectra of the chiral metasurface with $\alpha = 0.045$ and a 6° tilt in the positive y direction. Here, chiral CD is defined as the transmittance difference between different Jones matrix components under RCP and LCP incidence in circularly polarized bases [24,44,45]:

$$\text{CD} = \frac{(T_{ll} + T_{rl}) - (T_{rr} + T_{lr})}{(T_{ll} + T_{rl}) + (T_{rr} + T_{lr})}, \quad (1)$$

where r and l represent RCP and LCP plane waves, respectively. Here, T_{ij} ($i = l, r; j = l, r$) denotes the transmittance for polarization i relative to polarization j . The intrinsic chirality BIC results in high- Q resonances with a CD exceeding 0.99 and a linewidth of 1 nm. Typically, high CD in nonintrinsic chirality cases is attributed to large cross-polarization waves (T_{lr} and T_{rl}) [45,46]. This results in elliptically polarized outgoing light, while intrinsic chirality undergoes no polarization conversion. This implies that the metasurface reflects all incident RCP waves from one side as counterpropagating waves with the same polarization while remaining transparent to all incident LCP waves, as shown in Fig. 2(d). At this point, the metasurface acts as a perfect selectively chiral light reflector. Further support for this conclusion is provided by the reflection spectra regarding intrinsic chirality and the temporal coupled mode theory (see Secs. 1 and 2 in the Supplemental Material [47]). To quantify this copolarized transmission selectivity, we can introduce the

transmittance difference: $\Delta T = T_{ll} - T_{rr}$. At the C point, $\Delta T = 1$, which means that the C point can block specific circular polarization components (T_{ll} , T_{rr}). If there is polarization conversion on the geometrically nonchiral metasurfaces, ΔT will disappear. Figures 2(e) and 2(f) illustrate the multipole analysis (multipole moments formula detailed in Sec. 3 in the Supplemental Material [47]) in the Cartesian coordinate system for RCP and LCP normal incidence at the intrinsic chirality q-BIC. The resonance is primarily supported by magnetic dipole (MD) moments, as accurately identified by observing the electromagnetic field distribution in Fig. 2(c). However, notably, the multipole scattering intensity for RCP incidence is more than three order of magnitude higher than that for LCP incidence, indicating strong coupling for RCP and decoupling for LCP when interacting with the chiral metasurfaces.

Topological charge is closely related to polarization vortex singularities in momentum space, which can connect or map the topological properties of energy bands into the radiation field. For nondegenerate in-plane wave vectors $\mathbf{k}_{||} = (k_x, k_y)$ above the light line and below the diffraction limit, only the wave vectors $\mathbf{k}_{||}$ with the same in-plane orientation (zero-order Fourier components) are compatible with the radiation waves. The far-field radiation to the plane of polarization vectors is represented as [30,52]

$$d(\mathbf{k}_{||}) = \hat{x} \frac{\int \mathbf{E}_x(\mathbf{r}, \mathbf{k}_{||}) dS}{\int dS} + \hat{y} \frac{\int \mathbf{E}_y(\mathbf{r}, \mathbf{k}_{||}) dS}{\int dS}, \quad (2)$$

where $\mathbf{E}(\mathbf{r}, \mathbf{k}_{||})$ represents the polarized electric field of far-field radiation, and S is the scattering cross-section. The electronic Bloch eigenfunctions $d(\mathbf{k}_{||})$ of Γ -BICs in momentum space possess extraordinary topological properties. Their high-symmetry points are considered polarization singularities, manifesting as a polarization vortex center in the far field, inevitably carrying an integer topological charge. The topological invariant q is described as [30,33]

$$q = \frac{1}{2\pi} \oint_C d\mathbf{k}_{||} \cdot \nabla_{\mathbf{k}_{||}} \phi(\mathbf{k}_{||}). \quad (3)$$

Topological charge describes the number of times the polarization vector wraps around a polarization singularity, where C is a closed loop in $\mathbf{k}_{||}$ space that encircles the polarization singularity counterclockwise. The orientation angle $\phi(\mathbf{k}_{||}) = \frac{1}{2} \arg[S_1(\mathbf{k}_{||}) + iS_2(\mathbf{k}_{||})]$ describes the angle between the major axis of its polarization ellipse and the x axis, where S_i is the Stokes parameter of $d(\mathbf{k}_{||})$ (see definition of S_i parameters in Sec. 3 in the Supplemental Material [47]). Figure 3(a) illustrates the evolution of the eigenpolarization states in momentum space with perturbations α and φ . In the absence of geometric perturbation, a polarization vortex singularity (V point) associated with a BIC can be observed at the Γ point. The V point exhibits a cross-polarization cancellation, making the polarization ambiguous in the far field. The polarization vortex exhibits a circular distribution, with its center carrying a topological charge of $q = +1$. Once a perturbation α is introduced, breaking the in-plane inversion symmetry, the electromagnetic fields of the metasurface are perturbed. At this point, the V point ($S_0, S_1, S_2, S_3 = 0$) rapidly splits into two C points ($S_1, S_2 = 0$) carrying $q = +\frac{1}{2}$, distributed on

both sides and pointing along the k_y direction in k space. The $C+$ and $C-$ points represent the intrinsic RCP and LCP states, respectively. They strongly couple with circularly polarized light in free space in the far field. However, the splitting associated with the V point inevitably causes them to shift away from the Γ point, resulting in a lack of far-field directionality. Due to the split C points being away from the Γ point along the k_y direction, it can be inferred that the intrinsic chirality appears in a tilted manner along the y direction, according to the points of mutual coupling in k space. As shown in Figs. 3(b) and 3(c), keeping $\alpha = 0.045$ and introducing perturbation φ , the eigenpolarization pattern also moves with the structural tilt direction. It is noteworthy that this entire process satisfies the conservation of energy, with the total topological charge remaining constant. For α and φ at appropriate positions ($\alpha = 0.045$, $\varphi = +6^\circ$ and $\alpha = 0.045$, $\varphi = -6^\circ$), the $C+/C-$ points can be precisely positioned at the Γ point, with the ellipticity ~ 1 (details in Sec. 4 in the Supplemental Material [47]), thus achieving characteristic chiral BIC at the $C+/C-$ point. Figures 3(d) and 3(e) display the topological distribution of the orientation angle (ϕ) at the Γ -BIC and q-BIC points. The C and V points manifest as Stokes phase vortices. The V point has a $q = +1$ topological charge, simultaneously providing an optical phase vortex with $l = 2q = 2$ counterclockwise rotations around the V point. The C point has a $q = +\frac{1}{2}$ topological charge, providing an optical phase vortex with $l = 2q = 1$ counterclockwise rotation around the C point. The polarization vortex centers precisely correspond to the positions of the C and V points in momentum space. It is the intrinsic spin angular momentum with $l = 1$ of the $C+/C-$ points that manifests this extreme chirality, and the displacement of the C point by the tilted metasurfaces make this intrinsic chirality achievable.

Additionally, the σ_z symmetry of the system can be disrupted through external conditions (nonnormal incident circularly polarized light). Figures 3(f) and 3(g) display angle-resolved transmission spectra under perturbation ($\alpha = 0.045$, $\varphi = 0$), respectively, for RCP and LCP incidence. The direction of the incident light tilt corresponds to the k_y direction along the y axis. At this point, a certain angle forms between the incident plane and the mirror line perpendicular to the metasurfaces, also disrupting the σ_z symmetry of the system. In the k_y direction, the intrinsic polarization of the opposite helicity is maintained. The nature of optical chirality is determined by the degree of coupling between the eigenstates of different helicities and the circularly polarized light in free space. The metasurfaces selectively transmit circularly polarized light of opposite directions when incident angles for RCP and LCP are -4° and $+4^\circ$, respectively, confirming the presence of $C+$ and $C-$ points, validating the selective coupling of the C points to circularly polarized light. This also means that the CD response of the metasurfaces can be obtained by oblique incidence, and oblique incidence in the opposite direction will produce CD values with opposite signs.

The different tilting directions of the metasurfaces can cause the C points to shift in different directions. As shown in Figs. 4(a) and 4(b), they respectively display the transmission peak curves and CD spectra for RCP and LCP with different

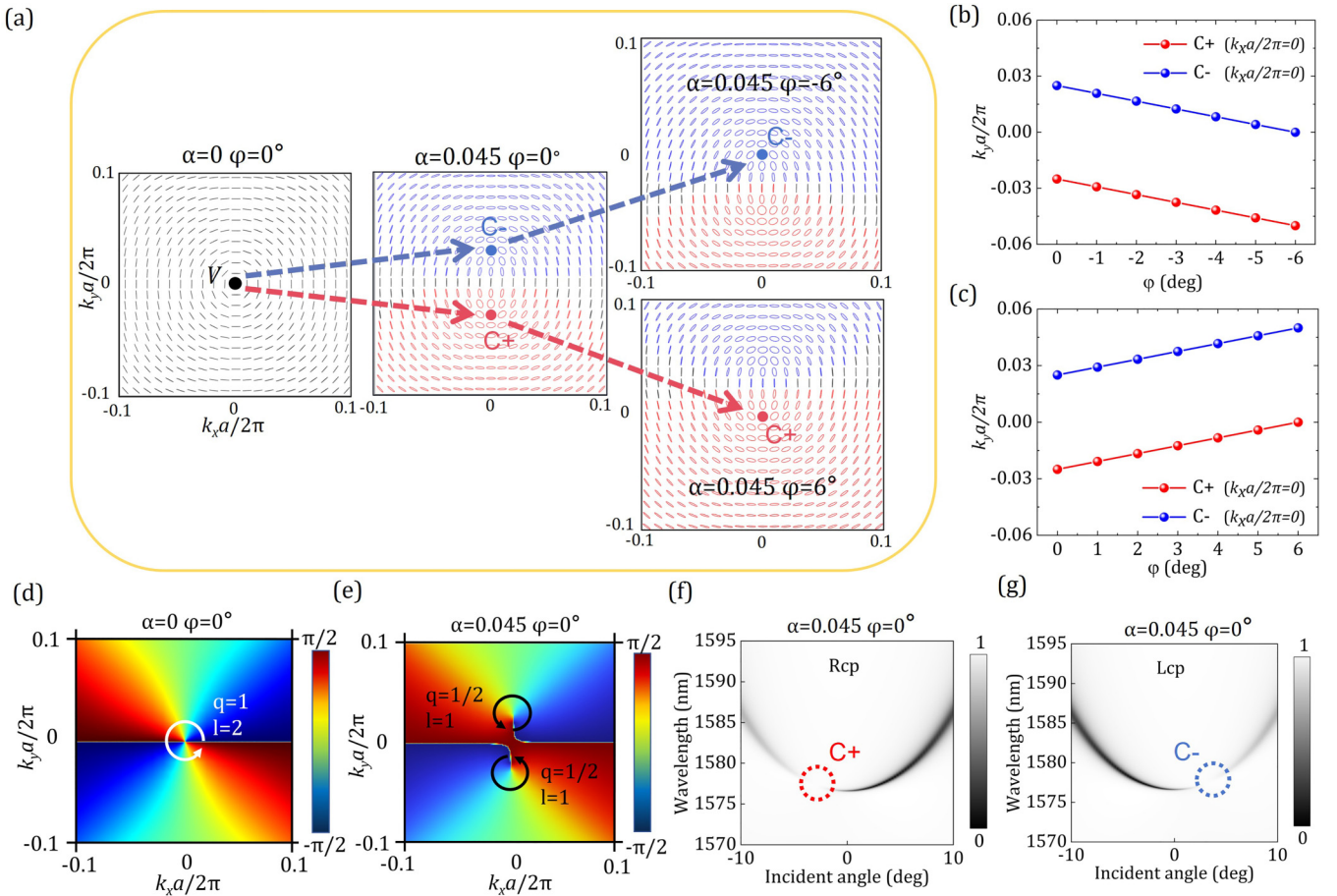


FIG. 3. (a) Eigenpolarization diagrams during the variation of metasurface parameters α and φ , where the blue and red ellipses represent left- and right-handed eigenpolarization states, respectively, and the black lines indicate the intrinsic linear polarization state. (b) and (c) Keeping $\alpha = 0.045$ constant, the relationship between the position of the C point in momentum space and the tilt angle φ . (d) Topological distribution of the orientation angle ϕ surrounding the V point with $q = +1$. (e) Topological distribution of the orientation angle ϕ surrounding the C point with $q = \frac{1}{2}$. (f) and (g) Under fixed geometric perturbation at $\alpha = 0.045$, angle-resolved transmission spectra of right-circularly polarized (RCP) and left-circularly polarized (LCP) light under nonnormal incidence are observed, encompassing $C+$ and $C-$ points.

perturbation parameters. This is consistent with the predicted evolution of the eigenpolarization states. When $\alpha = 0$ and $\varphi = 0$, the BIC state is completely embedded in the continuous spectrum, and the eigenstates are fully decoupled from all normally incident plane waves, resulting in no radiation loss. When $\alpha = 0.045$ and $\varphi = 0$, the V point splits into two C points with opposite helicities, but due to the presence of mirror symmetry in the z direction of the metasurfaces, there is no chiral response. The introduction of the parameter φ shifts the eigenpolarization states in the k space. When $\alpha = 0.045$ and $\varphi = +6^\circ$ ($\varphi = -6^\circ$), corresponding to the positions of $C+$ and $C-$ points in the Γ point, as shown in Fig. 3(a), they exhibit intrinsic RCP and LCP states in the far field, indicating that the metasurfaces flip the intrinsic spin-polarization states in opposite directions. Therefore, the asymmetric transmission of chiral fields can be observed for opposite metasurfaces tilt angles, with corresponding CDs approaching $+1$ and -1 , respectively. Figure 4(c) illustrates the relationship between the tilt angle of the metasurfaces and CD, with the maximum CD point precisely corresponding to the location of the C points near the Γ point. This indicates that the CD of the intrinsic chirality is governed and driven by

the half-integer topological charges. As demonstrated earlier, α follows the inverse quadratic law. Figure 4(d) shows that the Q factor is coherently controlled by dual perturbations (α and φ). Keeping α constant, the introduction of φ will further reduce the Q factor. Theoretically, if α and φ are kept within a small range, there is no restriction on the Q factor. When $\alpha = 0.045$ and $\varphi = +6^\circ$ ($\varphi = -6^\circ$), the Q factor reaches 5000 (neglecting material losses). Their coordinated changes also approximately follow the inverse quadratic law, allowing for different intrinsic chiral BICs with appropriate values of α and φ .

C. Nonlinear CD empowered by half-integer topological charges

As previously mentioned, q-BICs can induce significant electric field enhancement within the structure, providing a powerful platform for efficiently generating optical harmonics. Silicon is a material with strong third- and fifth-order nonlinearities (refer to polarization equations and conversion efficiency formulas in Sec. 6 in the Supplemental Material [47]). The local field strength at the third harmonic and fifth harmonic wavelengths depends on the enhancement

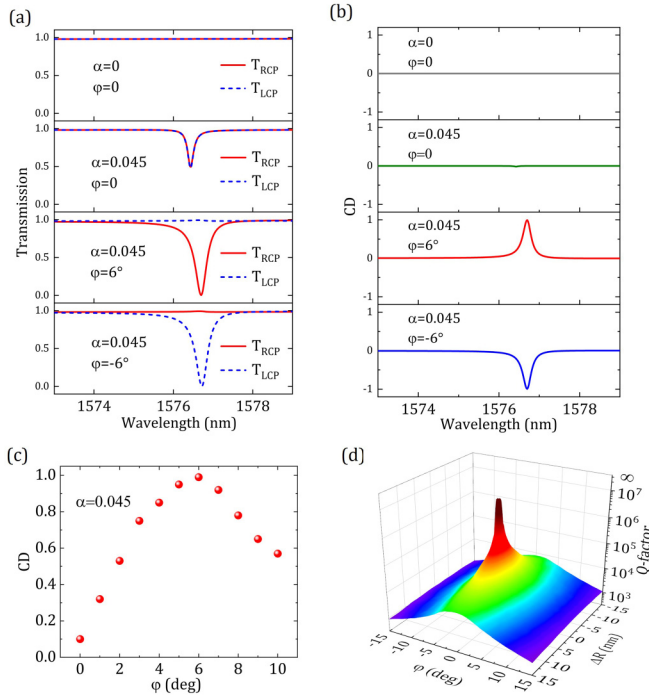


FIG. 4. (a) Transmission spectra of right-circularly polarized (RCP) and left-circularly polarized (LCP) light via introducing different asymmetry parameters ($\alpha = 0$, $\varphi = 0$; $\alpha = 0.045$, $\varphi = 0$; $\alpha = 0.045$, $\varphi = 6^\circ$; $\alpha = 0.045$, $\varphi = -6^\circ$). (b) Corresponding circular dichroism (CD) spectra. (c) Relationship between CD and tilt angle φ when $\alpha = 0.045$. (d) Q factor controlled by dual perturbation parameters (logarithmic scale).

of the fundamental frequency field strength [$I_{\text{loc}}^{(\omega)}$] and can be expressed as $I_{\text{loc}}^{(3\omega)} \propto [I_{\text{loc}}^{(\omega)}]^3$ and $I_{\text{loc}}^{(5\omega)} \propto [I_{\text{loc}}^{(\omega)}]^5$. Here, we primarily investigate the nonlinear CD of THG and FHG at the C point ($\alpha = 0.045$, $\varphi = 6^\circ$). For the metasurface in the opposite tilted direction, we can refer to the reverse case. Figure 5(a) illustrates that, at a pump power of $I_0 = 1 \text{ MW/cm}^2$, the energy of THG under RCP pumping is more than seven orders of magnitude higher than that under LCP pumping. Generally, higher-order nonlinear effects are weaker because the amplitude of high-order nonlinear effects is much smaller than that of low-order nonlinear effects, requiring a larger photon energy for excitation. Figure 5(b) shows the difference in FHG. The overall energy of FHG is seven orders of magnitude lower than that of THG. However, the energy of FHG under RCP pumping is more than 12 orders of magnitude higher than that of LCP pumping. Overall, the THG and FHG signals from LCP pumping are almost negligible.

Nonlinear CD can be defined as the difference in the total energy of optical harmonics generated under LCP and RCP pumping [53–55]:

$$\text{Nonlinear CD} = \frac{(I_{3\omega/5\omega}^{\text{RCP}} - I_{3\omega/5\omega}^{\text{LCP}})}{(I_{3\omega/5\omega}^{\text{RCP}} + I_{3\omega/5\omega}^{\text{LCP}})}. \quad (4)$$

Here, $I_{3\omega/5\omega}^{\text{RCP}}$ and $I_{3\omega/5\omega}^{\text{LCP}}$ represent the intensity of THG or FHG under RCP and LCP pumping, respectively. Due to the significant emission contrast of THG and FHG under RCP and LCP pumping, their nonlinear CD near the C point resonance is ~ 1 .

This near-perfect nonlinear CD reaches the theoretical maximum of chiral nonlinear dielectric metasurfaces [39,55,56]. Figure 4(a) also shows that, at $\alpha = 0.045$, $\varphi = +6^\circ$, the chiral metasurfaces exhibit a sharp resonance mode for RCP and an almost flat response for LCP incidence. This indicates the selective excitation of the q-BIC resonance for circularly polarized light, a feature determined by the eigenstates at the C point, resulting in nearly unitary nonlinear CD values. Figure 5(c) investigates the electric field distributions in the x and y directions for the resonance modes under RCP and LCP incidences, with insets showing the directions of their electric and magnetic fields, both excited by MD resonance. However, due to the opposite spin directions of incident photons in the $x - y$ plane, the distributions of E_x and E_y are completely opposite, and the directions of the electromagnetic field surrounding the MD resonance are also opposite. For RCP incidence, strong coupling exists, extremely enhancing the spin-correlated electric fields of E_x and E_y , with negligible enhancement of E_z . Conversely, it is decoupled for LCP incidence. The characteristics of this circularly polarized light selective coupling can be explained by the interaction of a pair of antiparallel dipoles [57]. Dual perturbations result in shifts in both in-plane and out-of-plane components of the dipoles (see Sec. 7 in the Supplemental Material [47]). Figure 5(f) reveals a significant contrast in near-field enhancement between RCP and LCP incidences, with the electric field enhancement for LCP incidence almost negligible. This is a crucial factor in achieving high nonlinear CD. Additionally, the scattered electromagnetic power of RCP and LCP in Figs. 2(e) and 2(f) also further emphasizes the strong correlation between the C point and significant near-field enhancement CD. Figures 5(d) and 5(e) show the double logarithmic relationship between the conversion efficiency of THG and FHG and the pump power. Based on the strong electric field confinement of q-BIC, the conversion efficiency of THG and FHG can be significantly improved, increasing with pump power. The conversion efficiency of THG differs by more than seven orders of magnitude between RCP and LCP pumping, while that of FHG differs by more than 11 orders of magnitude. The conversion efficiency of THG and FHG with respect to RCP and LCP pump powers follows a power-law growth relationship, characteristic of THG and FHG.

Figures 6(a) and 6(b) further investigate the evolutionary trajectory between near-field enhancement and the tilt angle of the metasurface. As the tilt angle of the metasurface gradually increases in different directions, the $C+$ and $C-$ points approach the Γ point in opposite directions along the Γ - Y axis. The metasurfaces exhibit selective shielding of near-field enhancement for LCP and RCP incident waves. When the C point is located at the Γ point ($\varphi = \pm 6^\circ$), it cannot be excited by far-field incident waves with spin-opposite circular polarization due to the spin selectivity of the intrinsic state. This imparts significantly intrinsic chirality to the metasurface, accompanied by substantial contrast in near-field enhancement, thereby enabling perfect nonlinear CD. On the other hand, we can also examine the near-field enhancement contrast induced by tilted incidence. Figure 6(c) shows the CD response resulting from tilted incidence while maintaining $\alpha = 0.045$ for the metasurfaces. Tilted incidence essentially involves the excitation coupling of non- Γ point intrinsic states. Due to the

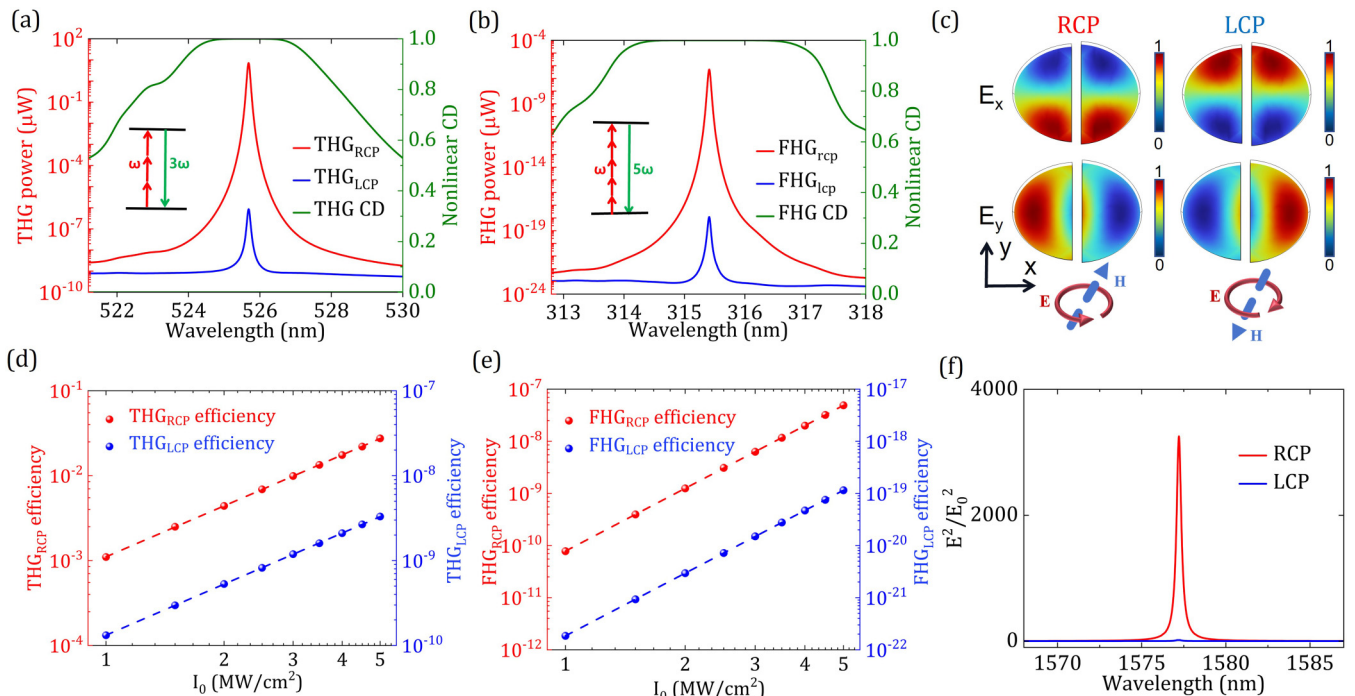


FIG. 5. (a) and (b) The intensity of third harmonic generation (THG) and fifth harmonic generation (FHG) at the C point under right-circularly polarized (RCP) and left-circularly polarized (LCP) incidences (logarithmic scale), respectively, with a fixed pump power $I_0 = 1$ MW/cm², along with their corresponding nonlinear circular dichroism (CD). The insets depict schematic illustrations of THG and FHG. (c) Distribution of E_x and E_y under RCP and LCP incidence, with corresponding schematic diagrams of magnetic dipole (MD) orientations shown in the insets. (d) and (e) Dependence of pump power and THG/FHG conversion efficiency (log-log scale). (f) At a fixed pump power of $I_0 = 1$ MW/cm², compare the near-field enhancement (E^2/E_0^2) in the metasurfaces for RCP and LCP incidences at the C point.

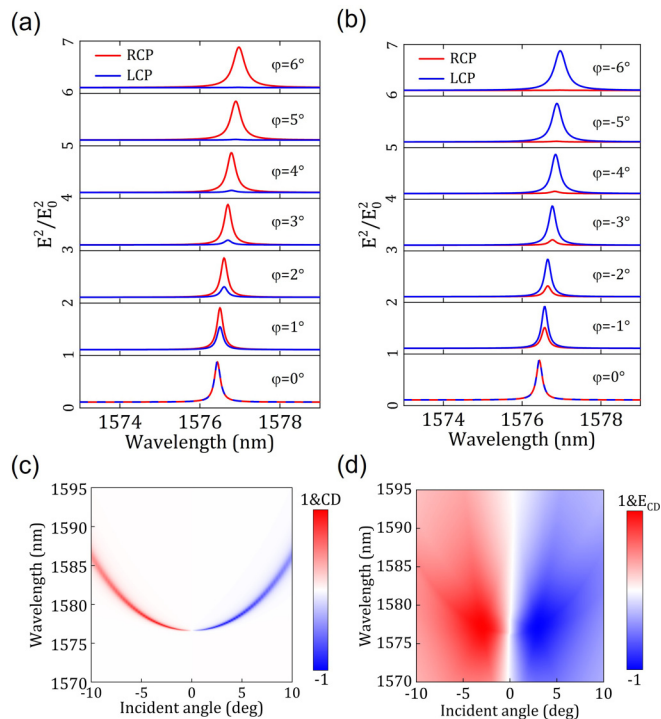


FIG. 6. (a) and (b) The evolution of near-field enhancement (E^2/E_0^2) with respect to the tilt angle φ under fixed $\alpha = 0.045$ for right-circularly polarized (RCP) and left-circularly polarized (LCP) incidences. (c) and (d) Linear circular dichroism (CD) and near-field enhancement CD resulting from tilted incidence.

splitting of the V point, the presence of the C point can be observed in opposite tilted incidences, exhibiting CD values with opposite signs at non- Γ point opposite tilted angles. The corresponding CD values reach their maximum with the tilt angles of -4° and $+4^\circ$, consistent with the observations in Figs. 3(f) and 3(g). At these angles, the C point couples with the incident light, acquiring extrinsic chirality. Figure 6(d) illustrates the near-field enhancement contrast resulting from circularly polarized light excitation under corresponding tilted incidence. Here, we introduce near-field enhancement CD: $E_{CD} = (E_{RCP}^2 - E_{LCP}^2) / (E_{RCP}^2 + E_{LCP}^2)$, where E_{RCP} and E_{LCP} are the electric field intensities under RCP and LCP incidences, respectively. The position of its maximum value is in basic agreement with the position of the maximum linear CD in Fig. 6(c), indicating the dependence of near-field enhancement CD on the C point. This further emphasizes the crucial role of the C point in achieving nonlinear CD. Shi *et al.* [24] achieved significant extrinsic chirality in planar chiral metasurface of double-sided scythe (DDS) architecture and realized nonlinear CD enhancement using the C point. Typically, the q-BICs resonance chirality in planar metasurface structures originates from nonreciprocity induced by the interaction between the mode and the substrate. However, in their investigations, the maximum linear CD resonance does not exhibit maximum nonlinear CD due to the presence of scattering background. Previous studies have also supported this viewpoint [39,40]. Here, using a tilted double-elliptical half-disk metasurface, we can simultaneously achieve perfectly linear CD and nonlinear CD at the C point, thanks to the

selective excitation of different spin circular polarizations during incidence.

III. CONCLUSIONS

In summary, we demonstrate a BIC metasurface platform that presents both linear and nonlinear chirality. Different from the previous extrinsic chirality that only introduced structural anisotropy or oblique incidence of light, our metasurfaces achieve dual symmetry breaking for both in-plane and out-of-plane symmetries by carefully customizing and tilting the resonators, precisely shifting the momentum-space C point to the Γ point. This imparts intrinsic chirality to the metasurfaces, enabling different spin selectivity by reversing the tilt direction. The metasurfaces realize nearly unitary CD (maximum CD > 0.99). Furthermore, benefiting from the high Q factor of the q-BIC and the electric field enhancement effect, it exhibits outstanding optical harmonic conversion efficiency. The C point possesses circularly polarized light

selective coupling characteristics, enabling the possibility of ultrahigh near-field enhancement contrast and nonlinear CD, with CD values ~ 1 for THG and FHG. Owing to the use of selective excitation of different spin circular polarizations, perfectly linear CD and nonlinear CD are therefore simultaneously achieved at the positions of half-integer topological charge. Otherwise, our approach is widely applicable and can find utility in various fields such as chiral light sources and nonlinear chiral optics, demonstrating remarkable flexibility and feasibility.

ACKNOWLEDGMENTS

This paper is funded by National Natural Science Foundation of China (Grants No. 62275112, No. 62065007, No. 11804134, and No. 11974188) and Natural Science Foundation of Jiangxi Province (Grants No. JXSQ2019201058, No. 09030030, and No. 20232ACB201009).

-
- [1] E. Plum, V. A. Fedotov, and N. I. Zheludev, Extrinsic electromagnetic chirality in metamaterials, *J. Opt. A: Pure Appl. Opt.* **11**, 074009 (2009).
- [2] P. Cintas, Chirality of living systems: A helping hand from crystals and oligopeptides, *Angew. Chem. Int. Ed.* **41**, 1139 (2002).
- [3] E. David and E. Carissa, *Health Systems Financing: The Path to Universal Coverage* (World Health Organization, Geneva, 2010).
- [4] Z. Wu, Y. Liu, E. H. Hill, and Y. Zheng, Chiral metamaterials via moiré stacking, *Nanoscale* **10**, 18096 (2018).
- [5] Z. Wang, F. Cheng, T. Winsor, and Y. Liu, Optical chiral metamaterials: a review of the fundamentals, fabrication methods and applications, *Nanotechnology* **27**, 412001 (2016).
- [6] I. Fernandez-Corbaton, M. Fruhnert, and C. Rockstuhl, Objects of maximum electromagnetic chirality, *Phys. Rev. X* **6**, 031013 (2016).
- [7] X. Luo, X. Du, R. Huang, and G. Li, High- Q and strong chiroptical responses in planar metasurfaces empowered by Mie surface lattice resonances, *Laser Photon. Rev.* **17**, 2300186 (2023).
- [8] J. Mun, M. Kim, Y. Yang, T. Badloe, J. Ni, Y. Chen, C.-W. Qiu, and J. Rho, Electromagnetic chirality: From fundamentals to nontraditional chiroptical phenomena, *Light Sci. Appl.* **9**, 139 (2020).
- [9] Z. Li, Y. Jiang, W. Liu, Y. Zhang, H. Cheng, J. Li, J. Tian, and S. Chen, Hybrid bilayer plasmonic metasurfaces with intrinsic chiral optical responses, *Appl. Phys. Lett.* **122**, 181702 (2023).
- [10] F. Lu, Y. Tian, M. Liu, D. Su, H. Zhang, A. O. Govorov, and O. Gang, Discrete nanocubes as plasmonic reporters of molecular chirality, *Nano Lett.* **13**, 3145 (2013).
- [11] C. Menzel, C. Helgert, C. Rockstuhl, E.-B. Kley, A. Tünnermann, T. Pertsch, and F. Lederer, Asymmetric transmission of linearly polarized light at optical metamaterials, *Phys. Rev. Lett.* **104**, 253902 (2010).
- [12] Q. Liu, M. Chao, W. Zhang, and G. Song, Dual-band chiral nonlinear metasurface supported by quasibound states in the continuum, *Ann. Phys.* **534**, 2200263 (2022).
- [13] A. Lininger, G. Palermo, A. Guglielmelli, G. Nicoletta, M. Goel, M. Hinczewski, and G. Strangi, Chirality in light-matter interaction, *Adv. Mater.* **35**, 2107325 (2023).
- [14] E. Plum, X.-X. Liu, V. A. Fedotov, Y. Chen, D. P. Tsai, and N. I. Zheludev, Metamaterials: Optical activity without chirality, *Phys. Rev. Lett.* **102**, 113902 (2009).
- [15] Y. Sun, Z. Hu, K. Shi, T. Guo, Y. Xing, Y. Jin, and S. He, Enhancing circularly polarized emission by a planar chiral dielectric metasurface, *Adv. Optical Mater.* **11**, 2300197 (2023).
- [16] J. H. Shi, Q. C. Shi, Y. X. Li, G. Y. Nie, C. Y. Guan, and T. J. Cui, Dual-polarity metamaterial circular polarizer based on giant extrinsic chirality, *Sci. Rep.* **5**, 16666 (2015).
- [17] Y. Chen, H. Deng, X. Sha, W. Chen, R. Wang, Y.-H. Chen, D. Wu, J. Chu, Y. S. Kivshar, S. Xiao *et al.*, Observation of intrinsic chiral bound states in the continuum, *Nature (London)* **613**, 474 (2023).
- [18] E. Plum, V. A. Fedotov, and N. I. Zheludev, Optical activity in extrinsically chiral metamaterial, *Appl. Phys. Lett.* **93**, 191911 (2008).
- [19] T. Cao, C. Wei, L. Mao, and Y. Li, Extrinsic 2D chirality: Giant circular conversion dichroism from a metal-dielectric-metal square array, *Sci. Rep.* **4**, 7442 (2014).
- [20] K. Tanaka, D. Arslan, S. Fasold, M. Steinert, J. Sautter, M. Falkner, T. Pertsch, M. Decker, and I. Staude, Chiral bilayer all-dielectric metasurfaces, *ACS Nano* **14**, 15926 (2020).
- [21] A. Y. Zhu, W. T. Chen, A. Zaidi, Y.-W. Huang, M. Khorasaninejad, V. Sanjeev, C.-W. Qiu, and F. Capasso, Giant intrinsic chiro-optical activity in planar dielectric nanostructures, *Light Sci. Appl.* **7**, 17158 (2017).
- [22] M. V. Gorkunov, A. A. Antonov, V. R. Tuz, A. S. Kupriianov, and Y. S. Kivshar, Bound states in the continuum underpin near-lossless maximum chirality in dielectric metasurfaces, *Adv. Optical Mater.* **9**, 2100797 (2021).
- [23] L. Kühner, F. J. Wendisch, A. A. Antonov, J. Bürger, L. Hüttenhofer, L. De S. Menezes, S. A. Maier, M. V. Gorkunov,

- Y. Kivshar, and A. Tittl, Unlocking the out-of-plane dimension for photonic bound states in the continuum to achieve maximum optical chirality, *Light Sci. Appl.* **12**, 250 (2023).
- [24] T. Shi, Z. Deng, G. Geng, X. Zeng, Y. Zeng, G. Hu, A. Overvig, J. Li, C.-W. Qiu, A. Alù, Y. S. Kivshar, and X. Li, Planar chiral metasurfaces with maximal and tunable chiroptical response driven by bound states in the continuum, *Nat. Commun.* **13**, 4111 (2022).
- [25] Q.-K. Liu, Y. Li, Z. Lu, Y. Zhou, W. M. Liu, X.-Q. Luo, and X.-L. Wang, Steerable chiral optical responses unraveled in planar metasurfaces via bound states in the continuum, *Phys. Rev. B* **108**, 155410 (2023).
- [26] H. Lee, A. Kecebas, F. Wang, L. Chang, S. K. Özdemir, and T. Gu, Chiral exceptional point and coherent suppression of backscattering in silicon microring with low loss Mie scatterer, *Elight* **3**, 20 (2023).
- [27] W. Chen, Q. Yang, Y. Chen, and W. Liu, Extremize optical chiralities through polarization singularities, *Phys. Rev. Lett.* **126**, 253901 (2021).
- [28] C. W. Hsu, B. Zhen, A. D. Stone, J. D. Joannopoulos, and M. Soljačić, Bound states in the continuum, *Nat. Rev. Mater.* **1**, 16048 (2016).
- [29] J. Jin, X. Yin, L. Ni, M. Soljačić, B. Zhen, and C. Peng, Topologically enabled ultrahigh- Q guided resonances robust to out-of-plane scattering, *Nature (London)* **574**, 501 (2019).
- [30] W. Liu, B. Wang, Y. Zhang, J. Wang, M. Zhao, F. Guan, X. Liu, L. Shi, and J. Zi, Circularly polarized states spawning from bound states in the continuum, *Phys. Rev. Lett.* **123**, 116104 (2019).
- [31] H. Qin, Z. Su, M. Liu, Y. Zeng, M.-C. Tang, M. Li, Y. Shi, W. Huang, C.-W. Qiu, and Q. Song, Arbitrarily polarized bound states in the continuum with twisted photonic crystal slabs, *Light Sci. Appl.* **12**, 66 (2023).
- [32] X. Yin, J. Jin, M. Soljačić, C. Peng, and B. Zhen, Observation of topologically enabled unidirectional guided resonances, *Nature (London)* **580**, 467 (2020).
- [33] W. Ye, Y. Gao, and J. Liu, Singular points of polarizations in the momentum space of photonic crystal slabs, *Phys. Rev. Lett.* **124**, 153904 (2020).
- [34] A. A. Bogdanov, K. L. Koshelev, P. V. Kapitanova, M. V. Rybin, S. A. Gladyshev, Z. F. Sadrieva, K. B. Samusev, Y. S. Kivshar, and M. F. Limonov, Bound states in the continuum and Fano resonances in the strong mode coupling regime, *Adv. Photon.* **1**, 016001 (2019).
- [35] Z. Liao, Q. Ma, L. Wang, Z. Yang, M. Li, F. Deng, and W. Hong, Guiding-mode-assisted double-BICs in an all-dielectric metasurface, *Opt. Express* **30**, 24676 (2022).
- [36] Z. Zheng, L. Xu, L. Huang, D. Smirnova, P. Hong, C. Ying, and M. Rahmani, Boosting second-harmonic generation in the LiNbO₃ metasurface using high- Q guided resonances and bound states in the continuum, *Phys. Rev. B* **106**, 125411 (2022).
- [37] X. Zhang, Y. Liu, J. Han, Y. Kivshar, and Q. Song, Chiral emission from resonant metasurfaces, *Science* **377**, 1215 (2022).
- [38] A. Overvig, N. Yu, and A. Alù, Chiral quasi-bound states in the continuum, *Phys. Rev. Lett.* **126**, 073001 (2021).
- [39] K. Koshelev, Y. Tang, Z. Hu, I. I. Kravchenko, G. Li, and Y. Kivshar, Resonant chiral effects in nonlinear dielectric metasurfaces, *ACS Photon.* **10**, 298 (2023).
- [40] M. Gandolfi, A. Tognazzi, D. Rocco, C. De Angelis, and L. Carletti, Near-unity third-harmonic circular dichroism driven by a quasibound state in the continuum in asymmetric silicon metasurfaces, *Phys. Rev. A* **104**, 023524 (2021).
- [41] W. T. Buono and A. Forbes, Nonlinear optics with structured light, *Opto-Electron Adv.* **5**, 210174 (2022).
- [42] A. Nikitina, A. Nikolaeva, and K. Frizyuk, Nonlinear circular dichroism in achiral dielectric nanoparticles, *Phys. Rev. B* **107**, L041405 (2023).
- [43] L. Fagiani, M. Gandolfi, L. Carletti, C. De Angelis, J. Osmond, and M. Bollani, Modelling and nanofabrication of chiral dielectric metasurfaces, *Micro Nano Eng.* **19**, 100187 (2023).
- [44] R. Wang, C. Wang, T. Sun, X. Hu, and C. Wang, Simultaneous broadband and high circular dichroism with two-dimensional all-dielectric chiral metasurface, *Nanophotonics* **12**, 4043 (2023).
- [45] Q. Duan, Y. Zeng, Y. Yin, J. Xu, Z. Chen, Z. Hao, H. Chen, and Y. Liu, Photonic crystal slabs with maximal chiroptical response empowered by bound states in the continuum, *Photon. Res.* **11**, 1919 (2023).
- [46] J. Li, Z. Yue, J. Li, C. Zheng, Y. Zhang, and J. Yao, Ultra-narrowband terahertz circular dichroism driven by planar metasurface supporting chiral quasi bound states in continuum, *Opt. Laser Technol.* **161**, 109173 (2023).
- [47] See Supplemental Material at <http://link.aps.org/supplemental/10.1103/PhysRevB.109.165420> for details, including the reflection spectra regarding intrinsic chirality and the temporal coupled mode theory; evolution of eigenstates under symmetric/asymmetric environmental refractive indices; multipole moments formula detailed; definition of parameters; polarization equations and conversion efficiency formulas; and electromagnetic near-field analysis of maximum chirality and chiral nonlinearity at point C. It also contains Refs. [48–51].
- [48] S. Fan, W. Suh, and J. D. Joannopoulos, Temporal coupled-mode theory for the Fano resonance in optical resonators, *J. Opt. Soc. Am. A* **20**, 569 (2003).
- [49] J. Wang, L. Shi, and J. Zi, Spin Hall effect of light via momentum-space topological vortices around bound states in the continuum, *Phys. Rev. Lett.* **129**, 236101 (2022).
- [50] S. Xiao, M. Qin, J. Duan, F. Wu, and T. Liu, Polarization-controlled dynamically switchable high-harmonic generation from all-dielectric metasurfaces governed by dual bound states in the continuum, *Phys. Rev. B* **105**, 195440 (2022).
- [51] D. J. Moss, E. Ghahramani, J. E. Sipe, and H. M. Van Driel, Band-structure calculation of dispersion and anisotropy in $\chi \rightarrow^{(3)}$ for third-harmonic generation in Si, Ge, and GaAs, *Phys. Rev. B* **41**, 1542 (1990).
- [52] T. Bai, Q. Li, Y. Wang, Y. Chen, Z.-D. Hu, and J. Wang, Terahertz vortex beam generator based on bound states in the continuum, *Opt. Express* **29**, 25270 (2021).
- [53] D. C. Hooper, A. G. Mark, C. Kuppe, J. T. Collins, P. Fischer, and V. K. Valev, Strong rotational anisotropies affect nonlinear chiral metamaterials, *Adv. Mater.* **29**, 1605110 (2017).
- [54] Q. Liu, B. Cheng, M. Chao, W. Zhang, Y. Xu, and G. Song, Giant nonlinear circular dichroism from high Q -factor asymmetric lithium niobate metasurfaces, *Ann. Phys.* **533**, 2100255 (2021).

- [55] K. Konishi, D. Akai, Y. Mita, M. Ishida, J. Yumoto, and M. Kuwata-Gonokami, Circularly polarized vacuum ultraviolet coherent light generation using a square lattice photonic crystal nanomembrane, *Optica* **7**, 855 (2020).
- [56] K. Frizyuk, E. Melik-Gaykazyan, J.-H. Choi, M. I. Petrov, H.-G. Park, and Y. Kivshar, Nonlinear circular dichroism in Mie-resonant nanoparticle dimers, *Nano Lett.* **21**, 4381 (2021).
- [57] M. V. Gorkunov, A. A. Antonov, and Y. S. Kivshar, Metasurfaces with maximum chirality empowered by bound states in the continuum, *Phys. Rev. Lett.* **125**, 093903 (2020).